Battery Health Management System for Automotive Applications: A retroactivity-based aging propagation study

Anirudh Allam, Simona Onori, *Member, IEEE,* Stefano Marelli, Carlo Taborelli

***Abstract*— Advances in lithium-ion battery technology have created new opportunities for this energy storage system to penetrate much deeper into the transportation sector, especially through automotive hybridization. In automotive applications, managing and optimizing the safety and reliability of batteries is of great interest for both users and manufacturers. To this purpose, battery management system (BMS) implements critical tasks such as monitoring battery health status, charge control, and cell balancing together with the evaluation of state of charge, state of health, and state of life. In this paper, we focus on BMS tasks related to the battery health management. We first cover main definitions, terminology and concept of batteries in automotive applications. An electrical-thermal-aging model of the battery cell is proposed, which is written in terms of fast (i.e. state of charge) and slow (i.e. state of health) dynamics. The time-scale separation of the proposed model is characterized quantitatively. A framework to analyze the propagation of aging from cell-to-cell within a battery pack is developed and the properties of an interconnected system from a degradation standpoint are studied. Further, a generalized framework for interconnected cells exhibiting the phenomenon of retroctivity is described. In addition, the effect of retroactivity and the extent of aging propagation are evaluated in a series and parallel topology, first and in a mixed series-parallel battery configuration later.**

I. Introduction

In response to the actual and future environmental and energy challenges worldwide, the automotive industry has been focusing on improving vehicle fuel efficiency. Although there is no silver-bullet technology to replace existing ones, at least in the near future, one possible answer to the challenges of future traffic is found in electrification of both the mobility and transport system. If, on one hand, many opportunities still exist to improve efficiency of conventional vehicles, vehicle electrification, today, seems like a promising path towards sustainable transportation. Consequently, new concepts and new technologies need to be developed to realize efficient electric vehicles suited for both individual and public mobility and for goods distribution in urban areas [1]. As shown in Fig. 1, a possible classification of today's vehicles in the market can be given based on internal combustion engine size and electric machine size [2], as follows:

1) Conventional internal combustion engine (ICE) vehicles;
2) Micro hybrids (start/stop);
3) Mild hybrids (start/stop + kinetic energy recovery+engine assist);

Anirudh Allam, Simona Onori (corresponding author), Stefano Marelli and Carlo Taborelli, are with the Automotive Engineering Department, Clemson University, Greenville, 29607, USA. {aallam, sonori, smarell, ctabore}@clemson.edu

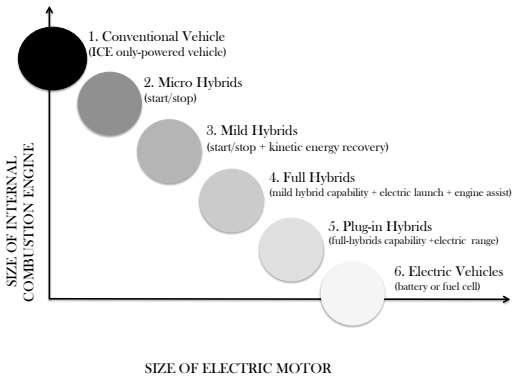

Fig. 1: Spectrum of vehicle technologies [2]: pathway of increasing electrification starting with ICE only-powered vehicles, going through different means of vehicle hybridization and ending up with pure electric vehicles powered by batteries or hydrogen fuel cell.

4) Full hybrids (mild hybrid capabilities + electric launch);
5) Plug-in hybrids (full hybrid capabilities + electric range) (PHEVs);
6) Electric Vehicles (EVs).

Batteries of all technologies are employed in all the different automotive applications listed above: from advanced lead-based batteries providing start-stop functionality and other micro-hybrid features, directly lowering fuel consumption by 5-10%, to high-voltage lithium-ion and sodium-nickel chloride batteries employed to deliver zero-emission driving in electric vehicles.

In particular, in PHEVs and EVs, high voltage battery systems are installed to provide significant levels of electric propulsion. Due to the need for high energy density, these vehicles are propelled predominantly by lithium-ion battery systems, which are additionally set apart by their fast recharge capability and good recharge and discharge power. They offer higher energy densities, long cycle life, and lighter weight than legacy battery chemistries such as nickel cadmium, nickel metal hydride and lead acid.

However, automotive applications are quite demanding as they place unprecedented cost, reliability, power/energy density, and safety requirements on electrochemical batteries. When managing and optimizing the safety and reliability of batteries, it is critical, for both users and manufacturers, to control cell balancing and evaluate state of charge, state of health, and state of life. These tasks are executed by the battery management system (BMS).

II. Challenges in Automotive Batteries

Comprehensive and mature BMSs are currently found in portable electronics, such as laptop computers and cellular phones, but they have not been fully deployed in EVs and HEVs. Batteries for PHEVs and EVs have to provide high voltage and high current. Moreover, the number of cells in a vehicles battery is hundreds of times greater than that in portable electronics and it is designed not only to be a long-lasting energy system, but also to be a high power system. Inevitably, designing BMSs for PHEVs and EVs is still a challenging task.

A BMS has to manage the tradeoffs among key performance parameters, like safety, life span, performance, specific energy, specific power, charging time and cost. Among those, an accurate quantification of the battery state is one of the most critical task for BMSs, along with the task of supervising lithium-ion cells when they are used in large battery packs.

Without a reliable battery management system the battery can get out of the so called safe operating area (SOA) which is bounded by the individual cell voltage, battery current and temperature limits specific to the battery chemistry. Getting out of the SOA can cause serious damages through thermal runaway of the battery or at least remarkably shorten the life of the battery.

In this paper we call Battery Health Management System (BHMS) the portion of BMS responsible to monitor and control the state-of-health (SOH) of a battery pack.

A battery cell delivers electric current as the result of an electrochemical reaction. Electrical current is carried by lithium-ions, from the positive electrode (cathode) to the negative electrode (anode) during charging, and from negative to positive during discharging. The ions are small and reside within the crystal structure of the electrode materials.

In hybrid and electric vehicles, a battery pack is composed of many cells (possibly hundreds) connected in series and parallel, usually in modules which are then connected to form a battery pack. Cells are wired in parallel to form a block to satisfy the requirement of high capacity while several blocks (or cells) are connected in series to provide a high voltage. Each cell is distinct due to manufacturing and chemical offset.

Within each module, each cell behaves differently due to manufacturing differences, aging, different operating temperatures, etc.. During charging, capacity fade in cells may result in danger if a cell comes to its full charge easily. When the battery consists of multi-cells in series, it will be subject to a higher failure rate than any single cell due to a series network. To reduce this effect and therefore prolonging battery life, an effective cell balancing mechanism that would keep the SOC level of individual cells in a battery pack as close to each other, must be developed. In addition to that, it is clear that understanding how much the failure rate of a cell increases upon interconnection, is an important issue to address as well. This is a fairly new research topic within the battery domain that is getting the attention of researchers today. In this paper, we propose a formal framework to tackle this problem.

III. Terminology of Battery Performance and Characterization

This section provides an introduction of the terminology used to classify, describe and characterize battery performance.

- *Battery Cell*. The smallest repeating unit of a battery. A cell contains an anode, cathode and electrolyte to deliver electric current as the result of an electrochemical reaction. The term battery is commonly applied to a single cell.
- *Battery module*. A group of interconnected electrochemical cells in a series and/or parallel arrangement, physically connected in an enclosure as a single unit to provide the required voltage and current levels.
- *Battery pack*. A completely functional system including battery modules, battery support systems and battery controls. A battery pack is the final energy storage assembly used in hybrid and electric vehicles.
- *Capacity*. It is the total charge that can be discharged from a fully charged battery under specified conditions (also referred to either Typical, Nominal, or Rated Capacity). Battery capacity Q_0 as a function of discharge current, $I(t)$ (positive current is used in discharge), is usually characterized by the Peukert equation

$$Q_0 = k\, I^n \tag{1}$$

  where n is the Peukert exponent and k is a fitting coefficient, [3].
- *State of Charge (SOC)*. This is a dimensionless value that describes the amount of usable charge that remains in the battery compared to the total charge capacity (under some nominal conditions). It can be expressed as:

$$SOC(t) = -\frac{\int_0^t I(\tau)d\tau}{Q_0} \times 100 \tag{2}$$

- *C-rate*. The C-rate is an expression describing the rate of charge or discharge current in normalized form:

$$C - rate = \frac{I}{Q_0}[1/h] \tag{3}$$

  The general expression is C/xx, where xx indicates the number of hours to completely discharge the battery at a constant current. For example, a rate of 5C will discharge the battery in $1/5$ hours ($= 12$ minutes), $C/1$ is the current at which the battery will last 1 hour. Hence, C/1 (or 1C) corresponds numerically to the battery nominal capacity in Ah.
- *Specific Energy*. Specific energy, also called gravimetric energy density, is used to define how much energy a battery can store per unit mass. It is expressed in Watthours per kilogram (Wh/kg). Specific energy of a battery is the key parameter for determining the total battery weight for a given mile range of EV.
- *Specific Power*. Specific power, also called gravimetric power density of a battery, is the peak power per unit mass. It is expressed in W/kg.

- *Energy Density*. Energy density, also referred as the volumetric energy density, is the nominal battery energy per unit volume (Wh/l).
- *Internal Resistance*. It indicates an overall resistance within the battery, generally different for charging and discharging, also dependent on the battery charge level.
- *Cut-off Voltage*. This is the minimum allowable voltage defined by the battery manufacturer. It is the voltage when discharge is complete.
- *Depth of Discharge (DOD)*. It is the percentage of battery capacity to which the battery is discharged.

$$DOD(t) = 1 - SOC(t) = \\ = -\frac{Q_0 - \int_0^t I(\tau)d\tau}{Q_0} \cdot 100 \qquad (4)$$

  The higher the DOD, the shorter the cycle life. To achieve a higher cycle life, a larger battery can be used for a lower DOD during normal operations.
- *State of Health (SOH)*. It can be defined as the ratio of the maximum charge capacity of an aged battery to the maximum charge capacity when the battery was new. SOH is an important parameter for indicating the degree of performance degradation of a battery and for estimating the battery remaining lifetime. For this reason, SOH definition is not univocal, because in a battery it can be defined by loss in capacity, increase in internal resistance, or a combination of both [4], [5]. Usually, SOH is correlated with the performance requirements which depend on the system and its specific application[1].
- *Calendar Life*. Calendar life is the expected life span of the battery under storage or periodic cycling conditions. It can be strongly related to the temperature and SOC during storage.
- *Battery Management System (BMS)*. It is a combination of sensors, controller, communication, and computation hardware with software algorithms designed to decide the maximum charge/discharge current and duration from the estimation of SOC and SOH of the battery pack.
- *Thermal Management System (TMS)*. It is designed to protect the battery pack from overheating and to extend its calendar life. Simple forced-air cooling TMS is adopted for the NiMH battery, while more sophisticated and powerful liquidcooling is required by most of the Li-ion batteries in EV applications.

IV. Battery aging

Real world systems are inherently subject to aging. Aging is the reduction in performance, availability, reliability, and life span of a system or component.

Aging originates from a number of different mechanisms and their interaction. These mechanisms are enhanced by stress factors such as load intensity, environmental conditions, and usage patterns. In a battery cell, aging includes capacity decrease, increase in cell impedance (which produces power fade), faster temperature rise during operation, lower voltage and more frequent self-discharge, all of which reduce battery performance. The physical-chemical mechanisms responsible for the aging are enhanced by stress factors such as current severity (C-rate), operating temperature (T_{batt}), state of charge, cycling rates, overcharge and over-discharge.

A review on today‘s knowledge on the aging phenomena in lithium-ion batteries can be found in [6].

Aging of lithium-ion cells is being more and more of a concern, as the battery-powered applications are very demanding, in that, they require the electrochemical system to last a very long life, sometimes exceeding 15 years. The batteries usually undergo two different types of aging: cycle life aging and calendar aging [7]. The capacity drop, in general, is due to parasitic side reactions, structural degradations, positive-electrode material dissolution, Solid Electrolyte Interface (SEI) layer formation and loss of contact between the electrode and the current collector [8]. In this paper, only the cycle life aging of the battery is considered for which two main families of modeling approaches have been proposed in the literature:

- *Electrochemical (physics-based) aging models*: these are physics-based models describing the actual phenomena of diffusion and charge transport of ions of lithium inside the battery. The main advantages of these models are their accuracy and applicability to simulate aging under different operating conditions. Their limitations, on the other hand, is in their need for a detailed knowledge of the aging mechanisms and the high CPU time. In the current literature, these type of models have been developed for different Li-ion battery chemistries [9], [10], [8], [11], [12]. However, the integration of these models inside a BMS for real time control is still a research question.
- *Semi-empirical aging models*: Typically these are phenomenological models developed from data obtained in a laboratory through large scale testing under different aging conditions. These type of models are developed without the need for knowledge of the aging process at the materials level. Although these models have low predictability as they only describe how the aging mechanisms manifests and do not capture their physics, they are good for control-oriented purposes as they require low computation time to predict degradation and can be easily integrated within a BMS [4], [13], [14], [15].

A. Aging propagation in large-scale systems

Large-scale systems are ubiquitous. By definition, a large-scale or complex system is composed of various inter-connected components [16]. The complexity of the behavior of a system increases with the increase in inter-connected components, and it becomes more challenging to monitor the functionality of the overall system when these components are exposed to disturbances, faults and aging.

[1]For instance, in HEV applications high power is required to provide adequate boost. In PHEV and EV applications the requirement is mileage range and therefore capacity to store energy. In PHEV applications, high power and large capacity to store energy are required.

In the case of batteries, life prediction deals with the entire battery system, and must include battery pack related effects, which are difficult to take into account if one only focuses on aging processes at the cell level [17].

Existing literature on aging modeling and SOH monitoring has so far been focused on individual components. The proposed work aims to understand the propagation of aging in interconnected systems. In this paper, we investigate the aging properties of isolated components upon interconnection. In particular, we analyze propagation of aging from cell-to-cell within a battery pack and state-of-health monitoring of battery pack based on the knowledge of its components (cells) and their aging interaction. This analysis is addressed in detail in Section VII.

B. Battery aging dynamics

It is common practice to model an engineering component subject to aging by the dynamic equations, [18],

$$\begin{cases} \dot{x} = f(x, \theta, u) \\ \dot{\theta} = \epsilon g(x, p) \end{cases} \tag{5}$$

where $x \in R^n$ is the set of state variables associated with the fast dynamic behavior of the component; $\theta \in R^p$ is the set of aging variables, i.e. the system parameters that change with the age of the component; ϵ is a positive scalar $\epsilon << 1$ representing the fact that the dynamics of the state variables are much faster than the dynamics of the aging variables; $u \in R^m$ are the external inputs acting on the component; $p \in R^q$ is the vector of the aging factors. The vector p can be composed of states and inputs or functions of these; $y \in R^l$ is the component output vector. The system described in (5) represents a singular perturbation model with slowly drifting parameters. As $\epsilon \downarrow 0$, the equations become

$$\begin{cases} \dot{x} = f(x, \theta, u) \\ \dot{\theta} = 0 \end{cases} \tag{6}$$

The dynamics of the speed-up system (6) in the fast time scale t shows that the aging variable θ is "frozen". With application to the isolated battery cell system, the vector of fast dynamics x is defined by $[SOC, T_{batt}]^T$ (^{T} indicates transpose), the vector of parameters θ is given by $[Q, R]^T$, the control signal is $u = P_{batt}$ and the output signal is simply V_{batt}. The vector p, referred to as severity factors vector, is given by $[SOC, T_{batt}, P_{batt}]$ and contains factors responsible to the battery aging. In the next section, the model of a battery cell is detailed in all of its three main components: electrical, thermal and aging; in Section VI a quantitative characterization of the different time-scales is investigated for a battery cell used in charge-sustaining HEV application.

V. Battery Cell Model

The battery cell model considered in this work is composed of three components: electrical, thermal and aging, as shown in Fig. 2. For each of these components, all the dynamics involved and their mutual effects are analyzed in this section.

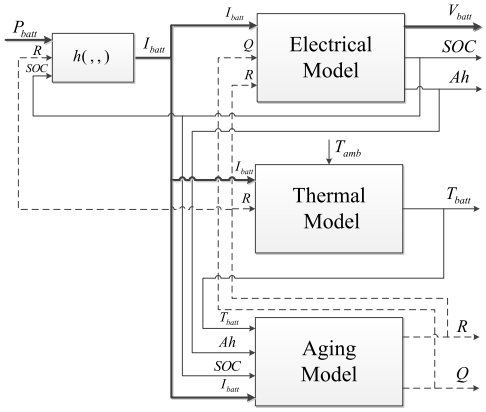

Fig. 2: Battery cell model layout showing the electrical, thermal and aging components

A. Electrical model

The electrical battery cell behavior is described with an equivalent 0^{th}-order model. The input to the battery cell is the power P_{batt}. The corresponding current is computed through the non-linear algebraic function $h(\cdot, \cdot, \cdot)$, which takes the form, [19]:

$$\begin{aligned} I_{batt} &= h(P_{batt}, SOC, R_0) = \\ &= \frac{V_{oc}(SOC) - \sqrt{V_{oc}^2(SOC) - 4R_0 P_{batt}}}{2R_0} \end{aligned} \tag{7}$$

where I_{batt} is the cell current (positive in discharge), V_{oc} is the open circuit voltage, which is a non-linear function of SOC, and R_0 is the cell internal resistance when the cell is new (BOL). R_0 is in general a function of SOC and the lumped internal temperature T_{batt}, *i.e.*, $R_0(SOC, T_{batt})$. Fig. 3 shows a typical trend of the resistance as a function of SOC parameterized for different values of temperature T_{batt}.

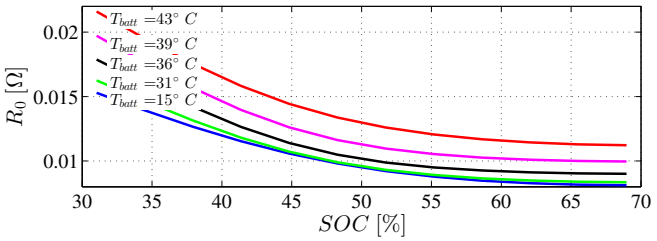

Fig. 3: Experimental characterization of R_0 as a function of SOC and T_{batt} for A123 ANR26650 battery cell

The cell SOC dynamics are defined by the equation:

$$\dot{SOC} = -\frac{I_{batt}}{Q_0 \cdot 3600} \tag{8}$$

where Q_0 is the capacity (in $[Ah]$) at BOL. Q_0 is a function of T_{batt} as shown in Fig. 4.

Note that the battery cell resistance R and the capacity Q are subject to a slow variation in time, starting from the initial (fresh) values R_0 and Q_0 respectively. As the battery is being used, the actual values of R and Q due to aging is described

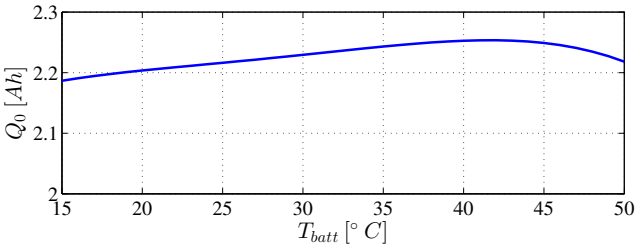

Fig. 4: Experimental characterization of Q_0 as a function of T_{batt} for A123 ANR26650 battery cell

in detail in Subsection V-C. The updated values R and Q, as they slowly vary over time, are used in (7) and (8) in place of R_0 and Q_0.

The output voltage V_{batt} is given by:

$$V_{batt} = V_{oc}(SOC) - R\, I_{batt} \tag{9}$$

B. Thermal model

The cell thermal model describes the cell temperature dynamics, taking into account the internal heat generation due to the current flowing inside the cell and the heat exchanged with the external environment. The dynamics of the internal temperature T_{batt} of the battery cell are described by:

$$\dot{T}_{batt} = \frac{1}{M_c C_p}\left[R\, I_{batt}^2 - \frac{T_{batt} - T_{amb}}{R_u}\right] \tag{10}$$

where $R\, I_{batt}^2$ is the thermal power generated by Joule effect, $M_c C_p$ is the effective cell heat capacity considered constant, T_{amb} is the ambient temperature and R_u is the thermal resistance to model the cell heat exchange with the environment. The values of the parameters of the first-order model used to simulate (10) are from [20].

C. Aging model

In this paper we model the aging dynamics, i.e. capacity decrease and resistance increase, by means of semi-empirical models identified over experimental data collected to mimic the battery behavior in a charge-sustaining HEV.

1) Capacity: We define the capacity loss of a cell as:

$$Q_{loss} = \frac{Q_0 - Q}{Q_0} \cdot 100 \tag{11}$$

where Q is the actual cell capacity subject to aging and $Q_0(T_{batt})$ is the capacity at BOL.

In this work, the Q_{loss} semi-empirical model considered is the one identified in [21] and expressed by the equation:

$$Q_{loss} = \sigma_{funct,Q}(SOC, I_c, T_{batt}) \cdot Ah^z \tag{12}$$

where $\sigma_{funct,Q}(SOC, I_c, T_{batt})$ is the *capacity severity factor function*, dependent on the *severity factors*, $[SOC, T_{batt}, I_c]$, (where $I_c = I_{batt}/Q$) and defined as:

$$\sigma_{funct,Q}(SOC, I_c, T_{batt}) = (\alpha_Q\, SOC + \beta_Q) \cdot e^{\left(\frac{-E_a + \eta_Q I_c}{R_{gas}(T_{batt}+273.15)}\right)} \tag{13}$$

and Ah is the Ampere-hour throughput whose dynamic equation is given by

$$\dot{Ah} = \frac{|I_{batt}|}{3600} \tag{14}$$

The capacity severity factor function (13) is an affine function of SOC, and an exponential function of I_c and T_{batt} (by means of the Arrhenius-type equation which is valid for temperatures above $15°C$ [22]). In (13) E_a is the activation energy and R_{gas} is the universal gas constant. The model was identified using experimental data from [23] and [24], collected over a state of charge range of $SOC \in [30\%, 70\%]$.

Since the experimental data used for the model identification are collected from tests conducted under constant condition of state of charge, C-rate and temperature, when computing the time derivative of Q, the capacity severity function ($\sigma_{funct,Q}$) is considered as constant, which leads to:

$$\frac{dQ}{dt} = \frac{\partial Q}{\partial Ah}\frac{\partial Ah}{\partial t}$$

Hence, the dynamics of the actual cell capacity, Q, is obtained from (11), (12) and (14) as a function of Q_{loss} and Q_0, and derived with respect to time as given in (15).

$$\dot{Q} = -\frac{Q_0}{100}\, \sigma_{funct,Q}(SOC, I, T_{batt})\; z\; Ah^{z-1}\frac{|I_{batt}|}{3600} \tag{15}$$

2) Resistance: The power fade process is characterized by the increase in internal resistance of the battery cell, defined in percentage as:

$$R_{inc} = \frac{R - R_0}{R_0} \cdot 100 \tag{16}$$

where R is the actual value of resistance in $[\Omega]$ and R_0 is its nominal value, corresponding to a fresh cell, as a function of both SOC and T_{batt}.

In literature, it is recognized that R_{inc} has a linear relation with Ah-throughput, according to a certain coefficient which takes into account the severity of the cycling conditions [22]. For the purpose of this work, a novel resistance increase model was identified from HEV aging data [25]. This model has the form:

$$R_{inc} = \sigma_{funct,R}(I_c, T_{batt}) \cdot Ah \tag{17}$$

where $\sigma_{funct,R}$ is the *resistance severity factor function* dependent on C-rate (I_c) and internal temperature (T_{batt}), defined as:

$$\sigma_{funct,R}(I_c, T_{batt}) = \left[\alpha_R + \mu_R\, e^{(\gamma_R\, I_c)}\right] \cdot e^{\left(\frac{-E_a}{R_{gas}(T_{batt}+273.15)}\right)} \tag{18}$$

The resistance severity factor function in (18) has an exponential dependence on I_c and has a typical Arrhenius term to take into account the dependence on T_{batt}. Its parameters have been identified based on the experimental data collected in [25]. There, the experimental campaign is performed at $T_{batt} = 55°C$, which determines the maximum temperature of validity of the model; while the minimum temperature is $T_{batt,min} = 15°C$. Further, the data is collected for the region of SOC from 0% to 30%. Three values of C-rate

were tested: $I_c = 2, 4, 8\ 1/h$, which provide the experimental points for the identification of $\sigma_{funct,R}(I_c, T_{batt})$ as shown in Table I.

TABLE I: Experimental points for the identification of $\sigma_{funct,R}(I_c, T_{batt})$ collected at $\overline{T}_{batt} = 55°C$

I_c $[1/h]$	$\sigma_{funct,R}$
2	0.0015831
4	0.0023786
8	0.0027499

The parameters of $\sigma_{funct,R}$ (α_R, μ_R and γ_R) are identified with a non-linear least-square algorithm and the results are shown in Table II. The accuracy of the model is evaluated with the statistical parameter R^2, which is 0.9939. The comparison between experimental data and the identified model is shown in Fig. 5.

TABLE II: Parameters of $\sigma_{funct,R}(I_c, T_{batt})$ resulting from the identification

Parameter	Value
α_R	297.0222
μ_R	−297.7760
γ_R	−0.4160

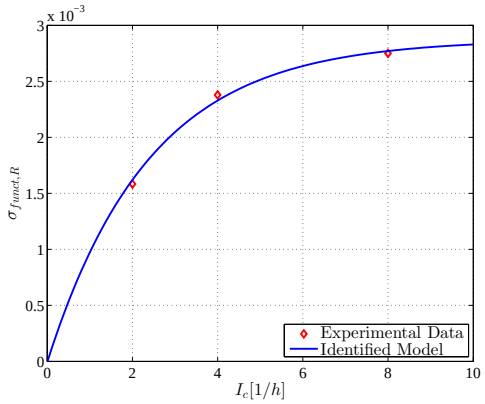

Fig. 5: Comparison between experimental data and the identified severity function $\sigma_{funct,R}(I_c, T_{batt})$

The dynamic equation for R is obtained by taking its derivative with respect to time, using (16), (17), and under the assumption of contant $\sigma_{funct,R}$, similar to the capacity loss dynamic equation.

$$\dot{R} = \frac{R_0}{100}\ \sigma_{funct,R}(I_c, T_{batt}) \cdot \frac{|I_{batt}|}{3600} \tag{19}$$

VI. Time Scale Separation

The battery cell model used in this paper is a dynamical system characterized by a time-scale separation. It is known that the electrical and thermal dynamics evolve over a different time-scale compared to the aging dynamics. However, this time-based separation behavior has never been formally studied in the literature, to the best of our knowledge. In this section, we aim to visualize the separation in time scale between the electrical, thermal and aging dynamics.

Every scale-separated dynamical system consists of a set of fast and slow variables. For a given input, the fast variables evolve quickly over time and reach a state of equilibrium; whereas the slow variables, during the same time, evolve very slowly. Hence, the evolution of the variables can be defined by the slope or its rate of change during the time taken by the fast variable to become stationary or stable. In other words, it could be said that the slope of a dynamic variable describes the time scale at which it evolves, and so a difference between slopes of two variables will reveal the separation in the time scale.

To that end, the equations for the rate of change of the fast and slow variables presented in the previous section are rewritten as follows:

$$\begin{cases} \dot{SOC} & = -\frac{I_{batt}}{Q \cdot 3600} = |m_{SOC}| \\ \dot{T}_{batt} & = \frac{1}{M_c C_p}\left[R\, I_{batt}^2 - \frac{T_{batt} - T_{amb}}{R_u}\right] = |m_{T_{batt}}| \\ \dot{Q} & = -\frac{Q_0}{100}\ \sigma_{funct,Q}(SOC, I, T_{batt})\ z\ Ah^{z-1}\frac{|I_{batt}|}{3600} \\ & = |m_Q| \\ \dot{R} & = \frac{R_0}{100}\ \sigma_{funct,R}(I_c, T_{batt}) \cdot \frac{|I_{batt}|}{3600} = |m_R| \end{cases} \tag{20}$$

where SOC, T_{batt} are the fast variables;Q, R are the slow variables and $m_{SOC}, m_{T_{batt}}, m_Q, m_R$ are defined to be the slope for the respective variables.

However, for the purpose of comparison of the evolution of the variables, we define the dynamics in (20) using the following formulism:

$$\dot{X} = |m_X| = \Psi_X \cdot m_{X,r}$$

where, $X = [SOC, T_{batt}, Q, R]$, Ψ_X is a dimensionless parameter defined as the rate of evolution of the dynamic variable, X, and $m_{X,r}$ is a unity gain with same dimensions as the slope m_X. In the same vein, we define the rate of evolution for all variables as follows:

$$\begin{cases} \dot{SOC} & = \Psi_{SOC} \cdot m_{SOC,r} \\ \dot{T}_{batt} & = \Psi_{T_{batt}} \cdot m_{T_{batt},r} \\ \dot{Q} & = \Psi_Q \cdot m_{Q,r} \\ \dot{R} & = \Psi_R \cdot m_{R,r} \end{cases} \tag{21}$$

The SOC is a fast variable and it is in the form of an integrator equation as given in (20). In order to have SOC reach a state of equilibrium, where $\dot{SOC} = 0$, we adapt the concept of working of an astable multivibrator. An astable multivibrator has two quasi-stable states and it oscillates between them, producing a constant square or rectangular waveform [26]. Quasi-stable state for a multivibrator is defined as the state in which the multivibrator will remain stable for a finite time, before it oscillates to another state. For that purpose, we define the operating range of SOC from 0.6 to 0.3. And in doing so, we impose two quasi-stable states on SOC, one at $SOC = 0.6$ and another at $SOC = 0.3$, such that, when SOC reaches any of these two states, the derivative of SOC ($\dot{SOC}$) will be equal to 0, thereby creating quasi-stability. This is achieved by subjecting the model to any constant discharge current until

$SOC = 0.3$, followed by a very short rest period of zero current, and then a constant charge current until $SOC = 0.6$, as shown in Fig. 6. Essentially, the SOC will oscillate, like an astable multivibrator, from one state to another and also remain stable in each state for a short period where the current is zero, as shown in Fig. 6. This approach allows us to see the dynamical equation of SOC in a new light, wherein it attains stability for a short period (when current is zero, $\dot{SOC} = 0$), allowing us to compute the rate of evolution of variables in the time taken by SOC to drop from 0.6 to 0.3 or rise from 0.3 to 0.6. The rate of evolution of all the variables, however, is not dependent on the direction of osciallation of SOC from one state to another, hence, in this paper, we only compute the rate of evolution during the time taken by SOC to drop from 0.6 to 0.3.

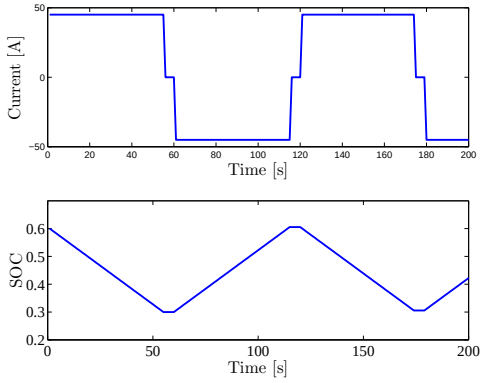

Fig. 6: a. Current profile; b. SOC profile

Further, the rate of evolution of the variables depends on the magnitude of current, initial battery temperature and the ambient temperature. Hence, we simulate (21) with a C-rate of varied magnitude, $I_c = [1, 5, 10, 20]\frac{1}{h}$, different initial battery temperatures, $T_{batt}(0) = [25, 30]^\circ C$, and a constant ambient temperature, $T_{amb} = 30^\circ C$.

When the magnitude of current is small and the initial T_{batt} is same as T_{amb} ($(T_{batt}(0) = T_{amb})$, the rate of evolution of T_{batt} ($\Psi_{T_{batt}}$) will be comparable to the rate of evolution of the slow variables (Ψ_Q and Ψ_R). This is considered as the worst case scenario wherein the time scales of the fast and slow variables will be the closest. For $T_{batt}(0) = T_{amb} = 30^\circ C$ and for a set of I_c values, the rate of evolution of all the variables are shown in Fig. 7 and Table III. Since the values of rate of evolution are of a very small order of magnitude, they are plotted using a logarithmic scale on the ordinate axis. From Fig. 7, it is observed that even for the worst case scenario, the rate of evolution $\Psi_{T_{batt}}$, Ψ_{SOC} differs from Ψ_Q and Ψ_R by more than two orders of magnitude.

Further, as the difference between the initial battery temperature and ambient temperature increases ($T_{batt}(0) \neq T_{amb}$), the thermal dynamics will evolve fast to become stable, and hence the rate of evolution $\Psi_{T_{batt}}$ will be always greater than Ψ_Q and Ψ_R. For $T_{batt}(0) = 25^\circ C$, $T_{amb} = 30^\circ C$ and for a set of C-rate values, the rate of evolution of all the variables are shown in Fig. 8. It is observed that

TABLE III: Rate of evolution for $T_{batt} = T_{amb} = 30^\circ C$ and $I_c = [1, 5, 10]\frac{1}{h}$

Rate of Evolution	$I_c = 1\frac{1}{h}$	$I_c = 5\frac{1}{h}$	$I_c = 10\frac{1}{h}$
Ψ_{SOC}	$2.77 \cdot 10^{-4}$	$1.28 \cdot 10^{-3}$	$2.76 \cdot 10^{-3}$
$\Psi_{T_{batt}}$	$1.03 \cdot 10^{-4}$	$1.00 \cdot 10^{-2}$	$6.26 \cdot 10^{-2}$
Ψ_Q	$8.95 \cdot 10^{-7}$	$6.04 \cdot 10^{-6}$	$1.79 \cdot 10^{-5}$
Ψ_R	$3.99 \cdot 10^{-11}$	$5.36 \cdot 10^{-10}$	$1.42 \cdot 10^{-9}$

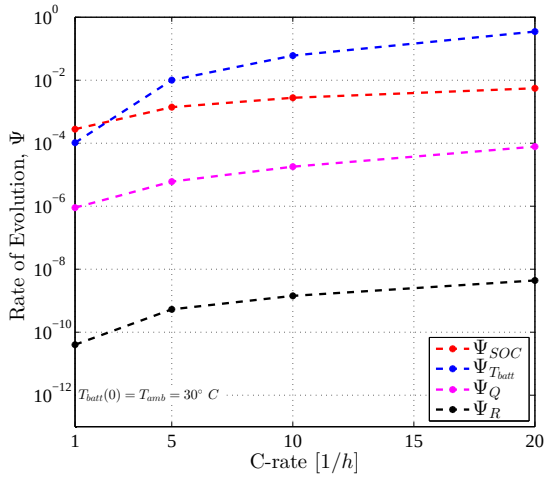

Fig. 7: Rate of Evolution for a range of C-rate values with initial $T_{batt} = 30^\circ C$ and $T_{amb} = 30^\circ C$

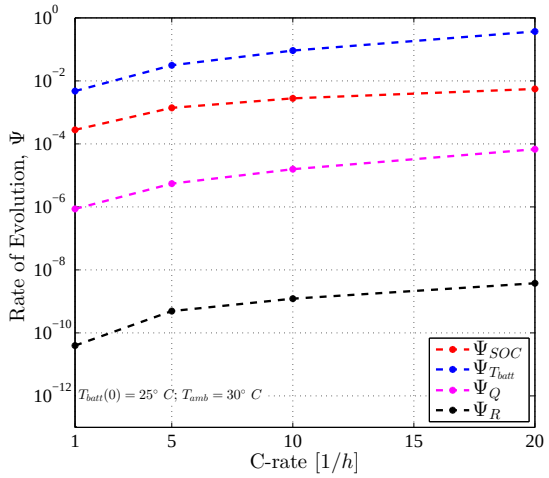

Fig. 8: Rate of Evolution for a range of C-rate values with initial $T_{batt} = 25^\circ C$ and $T_{amb} = 30^\circ C$

there is a broad separation between the rate of evolution of the fast and slow variables for even the smallest value of I_c.

Based on the above results, we conclude that the time scale separation between the fast and slow dynamics is not always constant and it depends on external factors. Mainly, for low values of C-rate, the time scale separation is highly dependent on the difference between the initial battery temperature, ($T_{batt}(0)$, and the ambient temperature, (T_{amb}, as witnessed in the difference in value of $\Psi_{T_{batt}}$ for $I_c = 1$ in Fig. 7 and 8. However, for higher C-rates, the time

scale separation no longer depends on the the temperature difference, as is evident from similar rate of evolution values of variables for $I_c > 10$ in Fig. 7 and 8.

VII. Aging Propagation

To understand whether the aging propagates among cells within an interconnected structure, we start by analyzing the simplest interconnected configuration, *i.e.* series, that cells can be arranged within a battery pack.

In a battery pack, the cells are connected both electrically (the same P_{batt} flows with the series) and thermically. In Fig. 9, the thermal connection between the cells is such that the temperature of cell i is affected by the temperature of the adjacent cells (both downstream $(i+1)$ and upstream $(i-1)$).

The property of modularity in a system guarantees that the input/output behavior of a component (a cell) does not change upon interconnection (series of cells) and the behavior of the interconnected system can thus be predicted by the behavior of the composing cells [27]. We want to show that there is no modularity in a battery pack, as far as aging goes, by demonstrating that the degradation of cell i is affected, indistinctly, by the degradation of the cell $i+1$ or $i-1$.

The interconnected system of Fig. 9 is characterized by electrical and thermal connections. If, on one hand, electrical modularity is guaranteed (from which the electrical behavior of the overall system can be inferred from the electrical behavior of the single cells), on the other hand, the thermal characterization of the interconnected system cannot be derived looking at the single cells. Because of that, also the aging of the interconnected series cannot be inferred by solely looking at the aging of the single cells.

The thermal dynamics of the connected cell i can be spelled out as follows:

$$\dot{T}_{batt,i} = \frac{1}{\tau_T}\left[R_i h(P_{batt})^2\right] - \frac{T_{batt,i} - T_{amb}}{R_u \cdot \tau_T} - \frac{T_{batt,i} - T_{batt,i-1}}{R_{c,i-1} \cdot \tau_T} - \frac{T_{batt,i} - T_{batt,i+1}}{R_{c,i+1} \cdot \tau_T} \quad (22)$$

where the thermal model introduced in Subsection V-B is completed with the addition of two heat exchanges with the adjacent cells. In particular, with reference to (10), R_i is the electrical internal resistance of cell i, $\tau_T = M_c C_p$ and the thermal resistances R_u and R_c represent respectively the thermal connection with the ambient and with the other adjacent cells.

Thus, (22) can be rewritten as:

$$\dot{T}_{batt,i} = \frac{1}{\tau_T}\Big[R_i h(P_{batt})^2 - T_{batt,i}\Big[\frac{1}{R_u} + \frac{1}{R_{c,i-1}} + \frac{1}{R_{c,i+1}}\Big] + \frac{T_{amb}}{R_u} + \boxed{\frac{T_{batt,i-1}}{R_{c,i-1}}} + \boxed{\frac{T_{batt,i+1}}{R_{c,i+1}}}\Big] \quad (23)$$

From (23), we see that thermal dynamics of cell i are determined by : 1) the current flowing into the cell i itself, 2) the external temperature T_{amb}, and 3) the temperature of the adjacent cells $T_{batt,i-1}$ and $T_{batt,i+1}$, represented in the boxed equations. Because of these two terms, modularity is lost, in the sense that the temperature of cell i changes upon interconnection, hence prediction of the thermal behavior of the system cannot be directly derived from the behavior of its components only. The two terms framed in the boxes in (23) can be interpreted as impedance-like effects that change the dynamics of the system (cell i) in the face of both downstream and upstream system [28]. From the standpoint of cell i, the term $\frac{T_{batt,i+1}}{R_{c,i+1}}$ accounts for the change in the system dynamics of cell i when it is connected to downstream system $i+1$. Symmetrically, the term $\frac{T_{batt,i-1}}{R_{c,i-1}}$ accounts for the change in the system i due to the interconnection with the system upstream.

Due to the nature of the thermal interconnection, from Fig. 10 we see that the aging in the component $i-1$ in term of increase of resistance ΔR_{i-1} propagates to the component i through the thermal dynamics of the cell $i-1$ and i leading to an increase of aging of the system i itself. This property is symmetrical with respect to the cell i, meaning that the same resistance increase in the cell $i+1$ will have the same impact, in terms of aging, to the cell i.

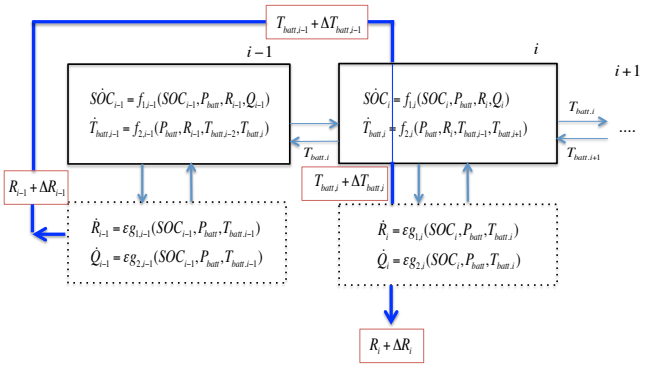

Fig. 10: Aging propagates from upstream cell $i-1$ to the downstream cell i.

VIII. Aging Propagation Framework

As shown in Section VII, the degradation in a cell will travel upstream as well as downstream in a system of interconnected cells. A first attempt to describe the aging propagation from an upstream cell to a downstream cell is found in [17], where the case of series configuration was studied for which a set of highly preliminary results was given. In this section, we aim to propose a more formal and exhaustive framework to explain analytically how the aging in a downstream cell will propagate to the upstream cell. In doing so, we borrow the theoretical framework based on retroactivity proposed by [27] to model interconnected systems composed of biological modules. Retroactivity, as described in [27], and adapted in the context of battery packs, is defined as the phenomenon in which a signal from a downstream cell affects the dynamics of an upstream cell.

Retroactivity signals within a battery pack are realized through the thermal coupling that exists between a downstream and an upstream cell (*i.e.* the term $\frac{T_{batt,i+1}}{R_{c,i+1}}$ from (23)) and they are primarily responsible for causing dissimilar aging of cells in a battery pack. For the purpose

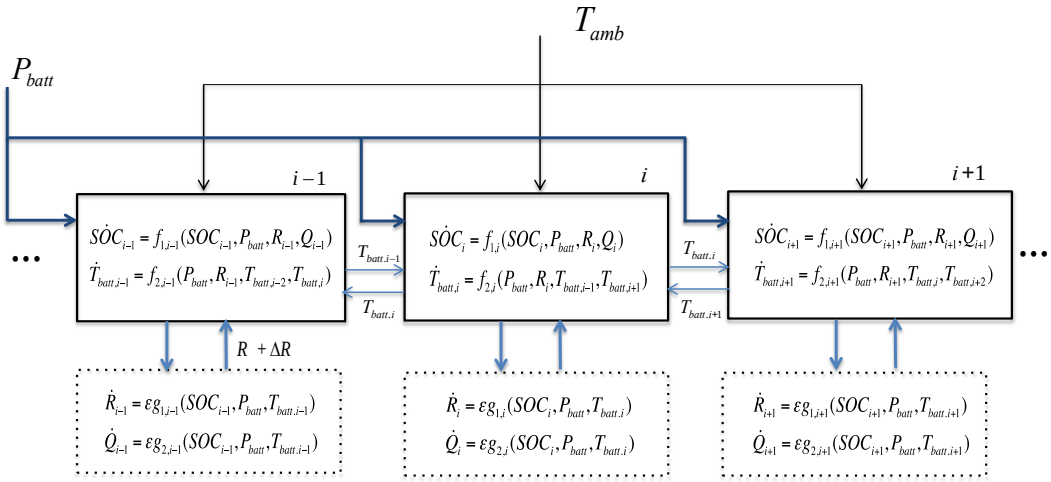

Fig. 9: Series interconnection of three cells.

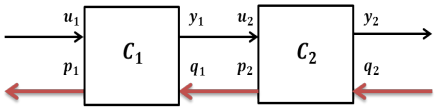

Fig. 11: Interconnected cells with the inclusion of retroactivity signals (in red).

of studying how aging propagates through retroactivity, we start considering two cells interconnected as in Fig. 11. The state-space representation of the two cells C_1 and C_2 and their interconnection (including retroactivity) is given by:

$$\begin{cases} \dot{x}_1 = f_1(x_1, \theta_1, u_1, q_1) & \dot{x}_2 = f_2(x_2, \theta_2, u_2, q_2) \\ \dot{\theta}_1 = \epsilon \cdot g_1(x_1, \theta_1, u_1, q_1) & \dot{\theta}_2 = \epsilon \cdot g_2(x_2, \theta_2, u_2, q_2) \\ y_1 = Y_1(x_1, u_1, q_1) & y_2 = Y_2(x_2, u_2, q_2) \\ p_1 = P_1(x_1, u_1, q_1) & p_2 = P_2(x_2, u_2, q_2) \end{cases} \tag{24}$$

where, x_i is the set of fast variables, θ_i is the set of aging variables, y_i is the output, p_i is the retroactivity signal to the upstream cell, q_i is the retroactivity signal from the downstream cell and $i = [1, 2]$. The diagram of Fig. 11 and equations (24) are easily generalizable to the case of interconnection of n cells. We define ξ_i as the *aging damage measure*, a scalar quantity that ranges from 0 to 1, signifying the progression of the aging process as

$$\xi_i = \frac{\theta_i - \theta_0}{\theta_f - \theta_0} \tag{25}$$

where, θ_0 is the initial condition of the aging variable when no aging has taken place, and θ_f is the value of the aging variable at the end of life [18].

To illustrate retroactivity, we consider the downstream cell, C_2, with a damage measure of ξ_2. We define the aging residual for the retroactivity signal p_2 of system C_2 as the difference of its output with aging, and its output with no aging [17], as

$$\Delta p_2 = p_{2,a} - p_2 = P_2(x_{2,a}) - P_2(x_2) = \phi(\xi_2) \tag{26}$$

Thus, we obtain that the residual of the retroactivity signal p_2 of system C_2 is an arbitrary function of its aging damage measure ξ_2. From the retroactivity framework in Fig. 11, it can be realized that the aging in C_2 is propagated to the upstream cell C_1 through retroactivity, as follows

$$q_1 = p_{2,a} = p_2 + \Delta p_2 = p_2 + \phi(\xi_2) \tag{27}$$

This results in the dynamics of the upstream system to be defined by

$$\begin{cases} \dot{x}_1 &= f_1(x_1, \theta_1, u_1, p_2 + \phi(\xi_2)) \\ \dot{\theta}_1 &= \epsilon \cdot g_1(x_1, \theta_1, u_1, p_2 + \phi(\xi_2)) \\ y_1 &= Y_1(x_1, u_1, p_2 + \phi(\xi_2)) \\ p_1 &= P_1(x_1, u_1, p_2 + \phi(\xi_2)) \end{cases} \tag{28}$$

It is clear from (28) that the dynamics and the output of the upstream system C_1 is altered due to the connection with the downstream system C_2. Hence, the aging of the upstream system is now dependent on aging of the downstream system, which transpires due to the presence of retroactivity. Furthermore, the residual of the retroactivity signal p_1 of system C_1 will affect the system that is upstream to C_1, thereby creating a chain of aging propagation through retroactivity.

IX. Aging Propagation in Series and Parallel Topologies

One reason for studying aging propagation is to understand what topology within a battery pack is least sensitive to the effects of retroactivity and therefore, more robust to the propagation of aging. In this section, we investigate the influence of retroactivity and evaluate the extent of aging propagation for two simple topologies, a string of *n* cells in series and a string of *m* cells in parallel. Further, we extrapolate the results obtained to comment on the aging propagation for a mixed (parallel-series) topology.

A. Sequence of aging propagation

1) Series: For a battery pack consisting of *n* cells in series, the current in the pack when subjected to a power

request of P_{pack} is given by:

$$I_{pack} = \frac{V_{oc,s}(\xi_Q) - \sqrt{V_{oc,s}^2(\xi_Q) - 4R_s(\xi_R)P_{pack}}}{2R_s(\xi_R)} \tag{29}$$

where,

$$\begin{cases} V_{oc,s}(\xi_Q) & = \sum_{i=1}^{n} V_{oc,i}(\xi_{Q,i}) \\ R_s(\xi_R) & = \sum_{i=1}^{n} R_i(\xi_{R,i}) \end{cases} \tag{30}$$

and $\xi_{Q,i}$ and $\xi_{R,i}$ are the aging damage measure variables for capacity and resistance of the form given in (25).
If one of the cells in the pack is more aged than the others, the resistance and voltage across the aged cell changes, resulting in an increased resistance of the pack, thereby drawing more current to satisfy the power request. The increase in current of the pack will increase the temperature of each cell. However, the temperature of the aged cell will increase more due to its higher resistance. Due to thermal interconnection, this increase in temperature of the aged cell affects the downstream and upstream cells, causing their temperature to increase more than usual. And since the aging dynamics are sensitive to the magnitude of current and temperature, an additional loss in capacity and increase in resistance in the downstream and upstream cells will occur.

2) Parallel: For a battery pack consisting of *m* cells in parallel, the current in the pack when subjected to a power request of P_{pack} is given by (31).

$$I_{pack} = \frac{V_{oc,p}(\xi_Q, \xi_R) - \sqrt{V_{oc,p}^2(\xi_Q, \xi_R) - 4R_p(\xi_R)P_{pack}}}{2R_p(\xi_R)} \tag{31}$$

where,

$$\begin{cases} V_{oc,p}(\xi_Q, \xi_R) & = \sum_{i=1}^{m} \dfrac{V_{oc,i}(\xi_{Q,i})}{R_i(\xi_{R,i})} \\ R_p(\xi_R) & = \dfrac{1}{\sum\limits_{i=1}^{m} \dfrac{1}{R_i(\xi_{R,i})}} \end{cases} \tag{32}$$

If one of the cells in the pack is more aged than the others, the resistance of the aged cell increases causing lower current to flow through it. Meanwhile, a high current is drawn by the entire pack to satisfy the power request. This results in additional load on the remaining cells, causing an increase in the flow of current into the branches parallel to the aged cell. The increasing current in the parallel branches causes an increase in their temperature. And since the aging dynamics are sensitive to the magnitude of current and temperature, an additional loss in capacity and increase in resistance in the downstream and upstream cells will occur.

In order to understand how the current varies with respect to the aging damage measure variables for both topologies, we simulate two battery packs, one with 5 cells in series and another with 5 cells in parallel, with only Cell 3 being aged, as shown in Fig. 12. We define *current residual* as the difference between current in the pack with an aged cell and the current in the pack with no aged cell as:

$$I_{pack,residual} = I_{pack,aged} - I_{pack} \tag{33}$$

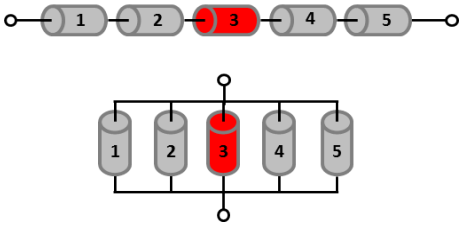

Fig. 12: Battery pack of 5 cells in a series and parallel topology with an aged Cell #3

A constant power request of 50 W is applied to the two battery packs shown in Fig. 12 and the current residual is plotted at the end of the simulation period of 700 seconds for varying aging damage measure variables (ξ_Q, ξ_R) as shown in Fig. 13 and 14. It is evident that current in the battery pack for both topologies is directly proportional to the aging damage measure variables (ξ_Q, ξ_R), meaning that as the cells degrades more, the current in the battery pack increases.

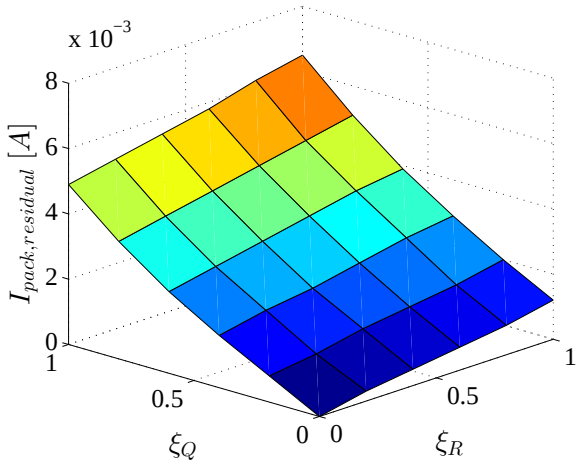

Fig. 13: Variation of current residual with respect to aging damage measure variables ξ_Q and ξ_R for a series topology

B. Retroactivity attenuation and quantification

In this subsection, we quantitatively investigate the effects of retroactivity in a series and parallel topology. We evaluate the severity of retroactivity by quantifying its influence on the capacity loss or resistance increase of cells downstream and upstream to the aged cell. For that purpose, we compare two the scenarios: 1) a battery pack exhibits retroactivity and, 2) retroactivity is attenuated, or in other words, the thermal coupling between cells in a battery pack is insulated.

Retroactivity attenuation is a broad field of research that will not be discussed in detail here. Retroactivity attenuation, with respect to battery packs, is insulation of the thermal interconnections, which can be achieved using active thermal management strategies like liquid cooling, air cooling or passive strategies like the usage of phase change materials [29]. These strategies absorb heat and maintain a uniform temperature throughout the battery pack.

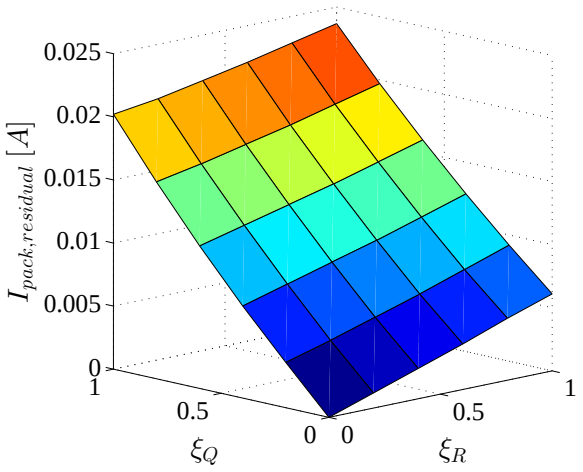

Fig. 14: Variation of current residual with respect to aging damage measure variables ξ_Q and ξ_R for a parallel topology

To quantify the effect of retroactivity on each cell, we define two retroactivity residual parameters for capacity loss and resistance increase, as follows:

$$\begin{cases} \zeta_{Q,i} = Q_{loss,r,i} - Q_{loss,nr,i} \\ \zeta_{R,i} = R_{inc,r,i} - R_{inc,nr,i} \end{cases} \tag{34}$$

where $Q_{loss,r,i}$ and $R_{inc,r,i}$ are the capacity loss and resistance increase of cell i in a battery pack exhibiting retroactivity, whereas $Q_{loss,nr,i}$ and $R_{inc,nr,i}$ are the capacity loss and resistance increase of cell i in a battery pack with no retroactivity. A constant power request of 50 W is applied to the two battery packs of Fig. 12 and the retroactivity residual parameters of all the cells are plotted at the end of the simulation period of 700 seconds.

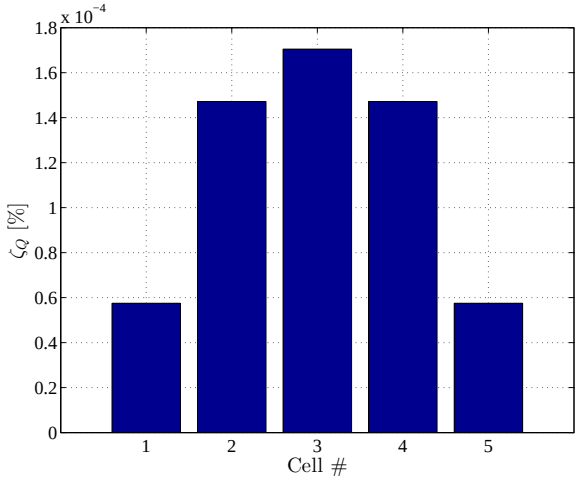

Fig. 15: Retroactivity residual for Capacity Loss (ζ_Q) for a series topology

In the case of a series topology, as shown in Figure 15 and 16, it can be observed that there is a noticeable effect of retroactivity on all 5 cells. There is a difference in retroactivity residual values between Cell #1 and Cell #2 showing that the cell closer to the aged cell is being affected more due

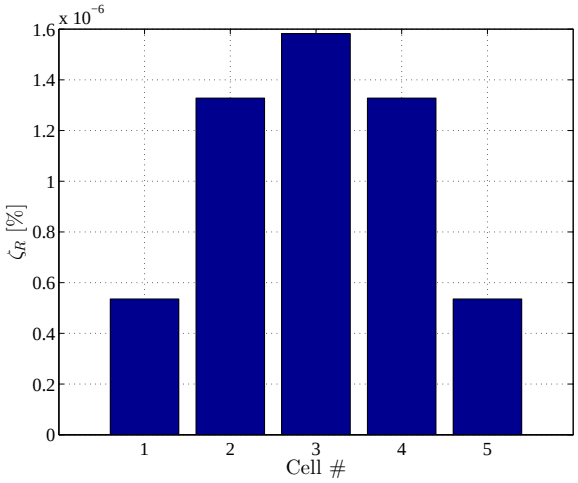

Fig. 16: Retroactivity residual for Resistance Increase (ζ_R) for a series topology

to retroactivity. Also, cells upstream and downstream to the aged cell (Cell #2 and #4), have equal retroactivity residual values, due to similar thermal interconnections, showing that they are equally affected by retroactivity. It is to be noted that as the duration of the usage of the battery pack increases, the retroactivity residual values for each cell will increase, causing certain cells to age sooner than they normally would.

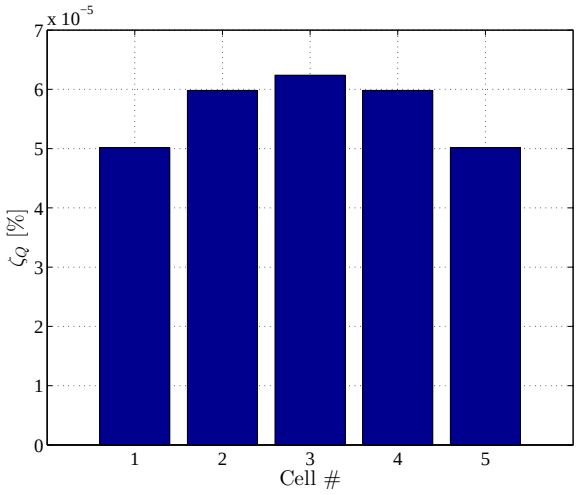

Fig. 17: Retroactivity residual for Capacity Loss (ζ_Q) for a parallel topology

For the parallel topology, as shown in Fig. 17 and 18, the difference in retroactivity residuals values between cells upstream and downstream to the aged cell is not as pronounced. More importantly, the retroactivity residual values are one order of magnitude lower than the values for a series topology, indicating that the effect of retroactivity is not dominant in a parallel topology. This is attributed to the low magnitude of current flowing through the aged cell which causes only a slight rise in its temperature. And since retroactivity manifests through thermal coupling, the resulting increase in temperature of the cells upstream and downstream to the aged cell is less. Hence, the aging

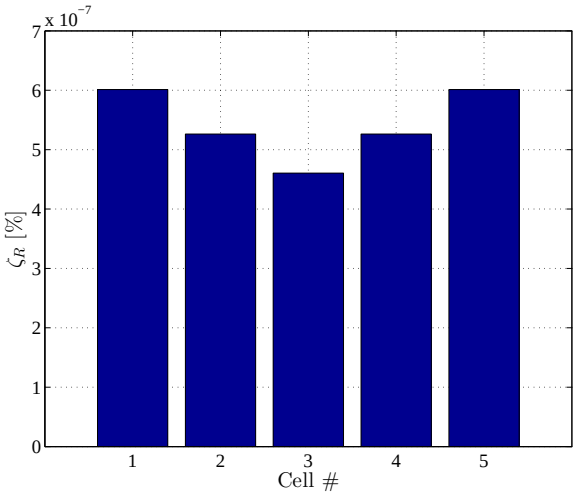

Fig. 18: Retroactivity residual for Resistance Increase (ζ_R) for a parallel topology

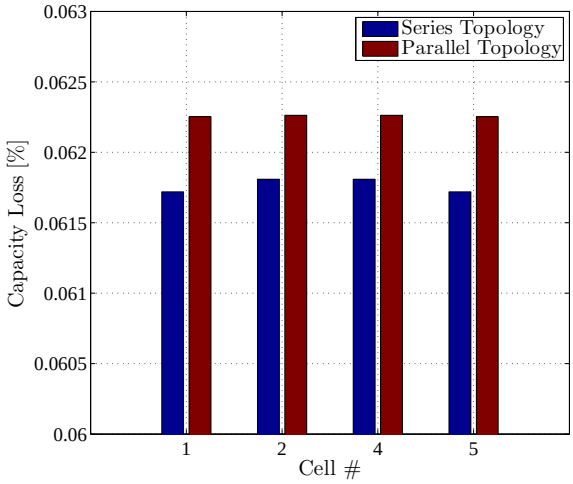

Fig. 19: Capacity Loss comparison between series and parallel topology

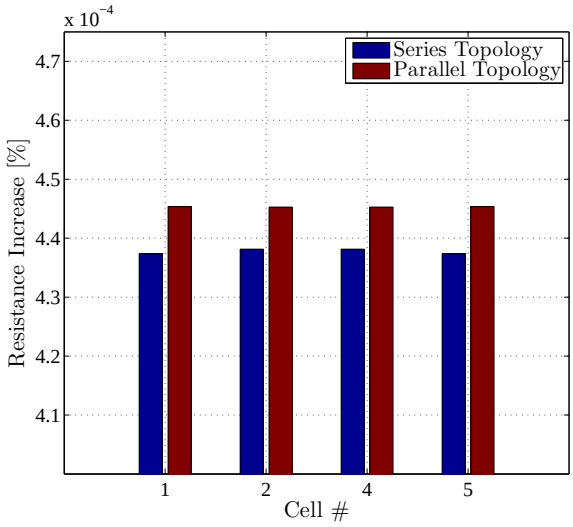

Fig. 20: Resistance Increase comparison between series and parallel topology

propagated through retroactivity in a parallel topology is not as severe as in the series topology.

C. Extent of aging propagation

We define the *extent of aging propagation* as the influence of an aged cell on the cells it is interconnected to. We evaluate the extent of aging propagation by comparing the capacity loss and resistance increase in cells in series and parallel with the aged cell, for a series and parallel topology respectively. A constant power request of 50 W is applied to the two battery packs in Fig. 12 and the capacity loss and resistance increase of all the cells (excluding the aged Cell 3, since we only want to observe the effect of aging on the interconnected cells) are plotted at the end of the simulation period of 700 seconds.

As observed in Fig. 19 and 20, the extent of aging propagation is higher in case of a parallel topology. Thus, a series topology is more robust to aging propagation. This is primarily attributed to the high magnitude of current flowing through the cells in parallel to the aged cell, due to which they degrade more.

In light of the above results, we can extrapolate and claim that in a mixed (parallel-series) configuration, the cells in series with the aged cell will degrade lesser than usual. To support this claim, we validate it by introducing an aged cell (Cell #3) in a topology combining series and parallel strings as shown in Fig. 21. We define capacity loss residual and resistance increase residual as follows:

$$\begin{cases} r_{Q,i} = Q_{loss,i,f} - Q_{loss,i,nf} \\ r_{R,i} = R_{inc,i,f} - R_{inc,i,nf} \end{cases} \tag{35}$$

where $Q_{loss,i,f}$ and $R_{inc,i,f}$ are the capacity loss and resistance increase of cell i in a battery pack with an aged cell, representing the faulty condition (f), whereas $Q_{loss,i,nf}$ and $R_{inc,i,nf}$ are the capacity loss and resistance increase of cell i in a battery pack with all cells fresh, representing the non-faulty condition (nf). A constant power request of 50 W is applied to the battery pack in Fig. 21 and the capacity loss and resistance increase residuals of all the cells are plotted at the end of the simulation period of 700 seconds.

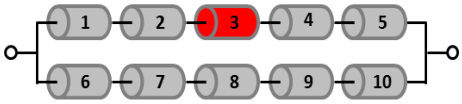

Fig. 21: Battery pack of 10 cells in a mixed (series-parallel) topology with an aged Cell #3

As claimed, the extent of aging propagation in the cells that are in series with Cell #3 is lower compared to the cells in parallel to Cell #3, as shown in Fig. 22 and 23. The negative residual values corresponding to the cells in series with Cell #3 indicate that they age lesser than they would normally do in the non-faulty scenario.

X. Conclusions and Future Works

In this paper, we addressed the topic of battery health management for automotive applications. In particular, the

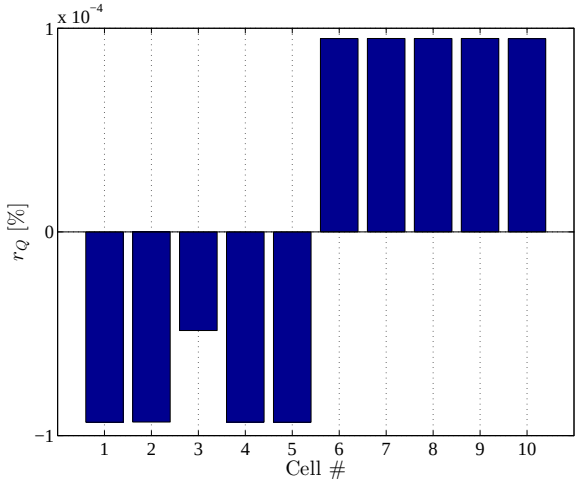

Fig. 22: Capacity Loss Residual of cells in a mixed (parallel-series) topology

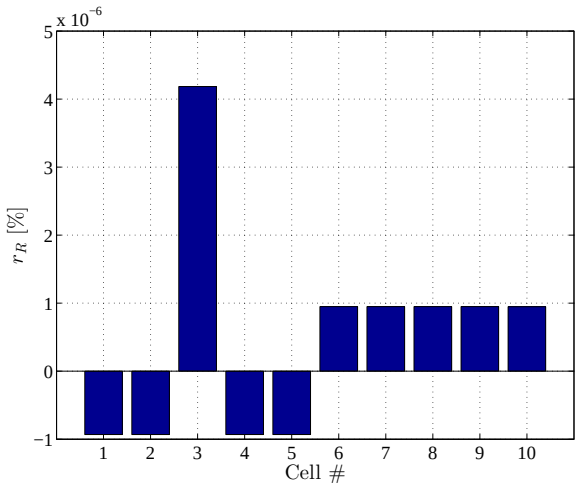

Fig. 23: Resistance Increase Residual of cells in a mixed (parallel-series) topology

battery cell aging and its propagation upon a battery pack configuration has been analyzed. Battery cell model has been described in terms of fast and slow dynamics, whose time-scale separation has been characterized quantitatively. A framework has been developed to describe the battery pack as an interconnected system, where propagation of cell degradation takes place. The phenomenon of retroactivity in battery packs is explored and a generalized framework showing degradation through retroactivity is developed. Further, the influence of retroactivity and the extent of aging propagation in a series and parallel topology is investigated. Finally, starting from an unbalance of the aging condition in a battery pack, represented as an aging fault injection in one cell, it is shown that the aging is propagating inside the pack, due to the coupling among the cells. As a result, a more aged battery pack has been achieved, where the cells closer to the aged one are affected more by the aging fault.

ACKNOWLEDGMENTS

The authors acknowledge the financial support of National Science Foundation through the GOALI Award #1301238.

REFERENCES

[1] C. C. Chan, "The state of the art of electric and hybrid vehicles," *Proceedings of the IEEE*, vol. 90, no. 2, pp. 245–275, 2002.

[2] A. A. Pesaran, "Choices and requirements of batteries for EVs, HEVs, PHEVs," in *NREL/PR-5400-51474*, April 2011.

[3] M. Jongerden and B. Haverkort, "Battery modeling," Enschede, January 2008. [Online]. Available: http://doc.utwente.nl/64556/

[4] S. Onori, P. Spagnol, V. Marano, Y. Guezennec, and G. Rizzoni, "A new life estimation method for lithium-ion batteries in plug-in hybrid electric vehicles applications," *International Journal of Power Electronics*, vol. 4, no. 3, pp. 302–319, 2012.

[5] K. Goebel, B. Saha, A. Saxena, J. R. Celaya, and J. P. Christophersen, "Prognostics in battery health management," *IEEE Instrumentation & Measurement Magazine*, vol. 11, no. 4, p. 33, 2008.

[6] J. Vetter, P. Novk, M. Wagner, C. Veit, K.-C. Mller, J. Besenhard, M. Winter, M. Wohlfahrt-Mehrens, C. Vogler, and A. Hammouche, "Aging mechanisms in lithium-ion batteries," *Journal of Power Sources*, vol. 147, pp. 269–281, Sep. 2005.

[7] M. Broussely, P. Biensan, F. Bonhomme, P. Blanchard, S. Herreyre, K. Nechev, and R. Staniewicz, "Main aging mechanisms in Li ion batteries," *Journal of Power Sources*, vol. 146, no. 1, pp. 90–96, 2005.

[8] M. Safari, M. Morcrette, A. Teyssot, and C. Delacourt, "Life-Prediction Methods for Lithium-Ion Batteries Derived from a Fatigue Approach: II Introduction: Capacity-Loss Prediction Based on Damage Accumulation," *Journal of The Electrochemical Society*, vol. 157, no. 6, pp. A713–A720, 2010.

[9] P. Ramadass, B. Haran, P. M. Gomadam, R. White, and B. N. Popov, "Development of First Principles Capacity Fade Model for Li-Ion Cells," *Journal of The Electrochemical Society*, vol. 151, no. 2, pp. A196–A203, 2004.

[10] S. Santhanagopalan, Q. Guo, P. Ramadass, and R. E. White, "Review of models for predicting the cycling performance of lithium ion batteries," *Journal of Power Sources*, vol. 156, no. 2, pp. 620 – 628, 2006.

[11] X. Lin, J. Park, L. Liu, Y. Lee, A. M. Sastry, and W. Lu, "A Comprehensive Capacity Fade Model and Analysis for Li-Ion Batteries," *Journal of The Electrochemical Society*, vol. 160, no. 10, pp. A1701–A1710, 2013.

[12] E. Prada, D. Di Domenico, Y. Creff, J. Bernard, V. Sauvant-Moynot, and F. Huet, "A Simplified Electrochemical and Thermal Aging Model of LiFePO4-Graphite Li-ion Batteries: Power and Capacity Fade Simulations," *Journal of The Electrochemical Society*, vol. 160, no. 4, pp. A616–A628, 2013.

[13] J. Wang, P. Liu, J. Hicks-Garner, E. Sherman, S. Soukiazian, M. Verbrugge, H. Tataria, J. Musser, and P. Finamore, "Cycle-life model for graphite-LiFePO4 cells," *Journal of Power Sources*, vol. 196, pp. 3942–3948, 2011.

[14] F. Todeschini, S. Onori, and G. Rizzoni, "An experimentally validated capacity degradation model for li-ion batteries in phev applications," *8th IFAC International Symposium on Fault Detection, Supervision and Safety of Technical Processes*, 2012.

[15] H. Wenzl, I. Baring-Gould, R. Kaiser, B. Y. Liaw, P. Lundsager, J. Manwell, A. Ruddell, and V. Svoboda, "Life prediction of batteries for selecting the technically most suitable and cost effective battery," *Journal of power sources*, vol. 144, no. 2, pp. 373–384, 2005.

[16] D. D. Siljak, *Large-scale dynamic systems: stability and structure*. North-Holland New York, 1978, vol. 310.

[17] S. Onori, G. Rizzoni, and A. Cordoba-Arenas, "A prognostic methodology for interconnected systems: preliminary results," in *8th IFAC International Symposium on Fault Detection, Supervision and Safety of Technical Processes, Mexico DF, Mexico*, 2012.

[18] L. Serrao, S. Onori, G. Rizzoni, and Y. Guezennec, "A novel model-based algorithm for battery prognosis," *Safeprocess*, 2009.

[19] L. Serrao, S. Onori, and G. Rizzoni, "ECMS as a realization of Pontryagins Minimum Principle for HEV control," *Proceedings of the 2009 American Control Conference*, 2009.

[20] A. Cordoba Arenas, S. Onori, Y. Guezzennec, and G. Rizzoni, "A control-oriented lithium-ion battery pack model for plug-in hybrid electric vehicles cycle-life studies and system design with consideration of health management," *Submitted to: Journal of Power Sources*, 2014.

[21] G. Suri and S. Onori, "A control-oriented Li-ion battery aging model for hybrid electric vehicle optimization," *Submitted to: Energy*, 2015.

[22] A. Cordoba Arenas, S. Onori, Y. Guezzennec, and G. Rizzoni, "Capacity and power fade cycle-life model for plug-in hybrid electric vehicle

lithium-ion battery cells containing blended spinel and layered-oxide positive electrodes," *Submitted to: Journal of Power Sources*, 2014.

[23] J. Groot, "State-of-health estimation of Li-ion batteries: cycle life test methods," *Licentiate thesis, Energy and Environment, Chalmers University of Technology, G oteborg, Sweden*, 2012.

[24] P. Spagnol, S. Onori, N. Madella, Y. Guezennec, and J. Neal, "Aging and characterization of Li-ion batteries in a hev application for lifetime estimation," *6th IFAC Symposium Advances on Automotive Control, Munich Germany*, July 12-14 2010.

[25] A. Suttman, "Lithium-Ion battery aging experiments and algorithm development for life estimation," *Master thesis, The Ohio State University Graduate Program in Mechanical Engineering*, 2011.

[26] P. Rao, *Pulse and Digital Circuits*. Tata McGraw-Hill Education, 2006, vol. 1.

[27] D. D. Vecchio, A. J. Ninja, and E. D. Sontag, "A System Theory with Retroactivity: Application to Transcriptional Modules," *Proceedings of the American Control Conference*, pp. 1368–1373, 2008.

[28] S. Jayanthi and D. D. Vecchio, "Retroactivity attenuation in bio-molecular systems based on timescale separation," *IEEE Trans. Aut. Control*, vol. 56, no. 4, pp. 748–761, 2011.

[29] G. Karimi and X. Li, "Thermal management of lithium-ion batteries for electric vehicles," *International Journal of Energy Research*, vol. 37, no. 1, pp. 13–24, 2012.